Optimizing Bundle Block Adjustment for High-Overlap Small-Format Multi-Head Camera Systems

Thirawat Bannakulpiphat[1,2,*], Wilfried Karel[1], Camillo Ressl[1], Norbert Pfeifer[1]

[1] Department of Geodesy and Geoinformation, Vienna University of Technology, Gusshausstraße 27-29, 1040 Vienna, Austria - (thirawat.bannakulpiphat, wilfried.karel, camillo.ressl, norbert.pfeifer)@geo.tuwien.ac.at

[2] Mapping and Positioning from Space (MAPS) Technology Research Center, Department of Survey Engineering, Chulalongkorn University, Bangkok 10330, Thailand

Technical Commission II

KEY WORDS: Multi-Head Camera Systems, Oblique Camera, UAV, Bundle Block Adjustment

ABSTRACT:

Small-format multi-head camera systems integrating nadir and oblique cameras are becoming standard in photogrammetry, offering the versatility needed for UAV-based mapping and surveying applications to collect high-quality data in challenging environments. A key consideration for these systems is the inherent limitations due to their small size, which may lead to various trade-offs, such as reduced ground coverage, overlap, and image quality, as well as constraints on using high-precision instruments like GNSS and INS. In this contribution, we propose the compass direction (CD) frame as a superior reference frame to avoid confusion regarding oblique cameras and oblique viewing directions. This approach supports continuous and consistent ground coverage, similar to the nadir camera, and facilitates easier analysis. We focus particularly on relative orientation, as it is a decisive factor for the consistency of subsequently derived information. We evaluate various influencing factors, including image connectivity, image ray intersection angle, and tie point multiplicity, in both single-camera (nadir) and penta-camera (nadir and oblique). The analysis reveals significant deviations in image connectivity from proportionality to image overlap. The percentage of overlap and side lap for nadir images influences the overlap for oblique cameras. While, there are no gaps at the near line between overlapping frames in each individual compass direction, the nadir images overlaps do not result in the same symmetry in the oblique image overlaps. Achieving such symmetry could enhance the visibility of facades in oblique images. In terms of the image ray intersection angle, the maximum intersection angles per tie point are well below the theoretical maximum, indicating a moderate exploitation of the accuracy potential offered by oblique images. Furthermore, analysis of the RMS error suggests that by adding the oblique images to the nadir image block and removing the 2-fold tie points, vertical accuracy improved considerably, while planimetric accuracy remained consistent.

1. INTRODUCTION

The use of aerial methods, including airplanes and Unmanned Aerial Vehicles (UAVs), for mapping and surveying has become increasingly popular due to their convenience and efficiency, particularly with the advancements in payload technologies such as multi-head camera systems. Multi-head, or oblique cameras are of particular interest because they provide more comprehensive coverage of complex environments, capturing images from multiple angles that enhance 3D modeling and improve the accuracy of mapping in urban and other detailed settings to support various smart city applications (Remondino and Gerke, 2015, Toschi et al., 2017). With the increasing use of UAVs, these systems offer significant advantages, including greater flexibility and reduced operational costs (Nex et al., 2022).

Traditionally, camera formats are categorized by sensor size into large, medium, and small formats. Large-format cameras, such as those from Vexcel Imaging and Leica, have large sensors offering resolutions over 100 MP. These cameras are ideal for aerial photography and mapping, where high resolution and large coverage are essential. Medium-format cameras (Phase One, Hasselblad, etc.) have sensors around 6 cm x 6 cm and resolutions between 50 MP and 100 MP, making them suitable for detailed aerial imaging and mapping projects that require high-quality images. Small-format cameras, including models from Canon, Nikon, Sony, etc., use 36 mm x 24 mm sensors and typically offer resolutions from 20 MP to 60 MP. While these cameras are more commonly used for general photography, they are also employed in aerial mapping when weight and size constraints are a concern. The "small-format" cameras in this study are even more compact, using APS-C sensor formats (around 24 mm by 15 mm), specifically designed for use on UAVs, where minimizing weight and size is critical for efficient and effective aerial surveying and mapping tasks.

Newly established small-format multi-head systems open up new possibilities by combining the advantages of oblique imaging with the lightweight and versatile nature of UAVs, enabling high-quality data collection even in challenging environments.

1.1 Motivation

The growing use of small-format multi-head camera systems in UAV-based mapping and surveying applications has highlighted the need to evaluate various computational factors that influence their performance and the quality of derived products. A key reason for these evaluations is the inherent limitations posed by the compact size of the systems. This may cause different trade-offs w.r.t. ground coverage, overlap, or image quality. Unlike larger, metric and more robust camera systems that can be equipped with high-quality INS (Inertial Navigation

Systems) and GNSS (Global Navigation Satellite Systems), the small-format systems used with UAVs are too light to support such heavy, high-precision instruments. Instead, these cameras typically rely on low-quality GNSS data and lightweight or no INS at all, resulting in reduced accuracy of single images in direct geo-referencing. Because of these constraints, it becomes essential to employ bundle block adjustment techniques. This method is crucial for providing good relative orientation within the block and ensuring the precision of the models derived. Additionally, it helps to guarantee overall accuracy by utilizing ground control points to compensate for low GNSS quality. This necessity drives the focus of our study on optimizing image processing workflows to enhance the quality of mapping and 3D reconstructions.

Key factors that affect the performance of these systems include the number and distribution of ground control points, the multiplicity and distribution of tie points, the type of camera processing (such as single-camera (nadir), penta-camera (nadir and oblique), which involves using images from different subsets of cameras only), and variations in land use across the surveyed area. Within this overall aim, we concentrate especially on relative orientation, as it is a decisive factor for the quality of subsequently derived information. We specifically investigate image connectivity, image ray intersection angle, and tie point multiplicity, focusing on the factors most critical to optimizing workflows. Our goal is not only to improve the precision and accuracy of bundle block adjustment but also to enhance other essential aspects such as reliability, automation, completeness, and production speed, ultimately leading to superior 3D reconstructions and mapping outcomes.

1.2 Related Work

Previous research has largely concentrated on the mathematical modeling and performance assessment of large-format multi-head camera systems used in manned aircraft (Verykokou and Ioannidis, 2020, Maset et al., 2024). However, applying these models to small-format systems designed for UAVs is an emerging field that demands further exploration. (Alsadik et al., 2022) made progress by validating a UAV hybrid sensor system consisting of five small-format RGB cameras and a LiDAR sensor, configured in a Maltese cross arrangement. This study demonstrated the potential of the system for 3D mapping, yet highlighted the need for future research to optimize flight planning and enhance data processing techniques. Similarly, (Bannakulpiphat and Santitamnont, 2024) examined the variations in camera rig parameters across different photogrammetric software platforms for the "FOXTECH 3DM-V3" small-format multi-head camera system. Their findings underscored the critical need for further optimization of camera rig parameters and the development of more advanced mathematical models to better align theoretical models with real-world configurations, ultimately aiming to improve photogrammetric accuracy.

It can be seen that there is ongoing research focusing on optimizing and developing small-format camera systems to enhance their output; however, additional research is still required to address various challenges specific to these types of sensors. As multi-view cameras for UAV platforms become more widely accessible, these studies collectively emphasize the importance of addressing the gaps in computational factors and modeling techniques, which are essential for achieving optimal outcomes in UAV-based photogrammetry.

1.3 Terminology

This study utilizes a "JOUAV CA502R" small-format multi-head camera system, consisting of one nadir and four 45-degree oblique cameras. At each exposure point, these cameras simultaneously capture five images, collectively referred to in this paper as a "penta group." Due to the design of the small-format multi-head camera system, specific codes are assigned to each camera by the manufacturer, depending on the position where the camera is mounted: the downward-looking (nadir) camera is labeled 'S', the camera mounted on the left 'A', the camera on the right 'D', the camera at the back 'X', and the camera at the front 'W'. Notably, these labels align with keys on the standard English keyboard layout, facilitating intuitive switching between cameras. This directional relationship is referred to as the *platform direction (PD)*, representing either the specific codes assigned by the manufacturer for each camera position (A, D, S, W, X) or the viewing direction (R, L, N, F, B). However, communication difficulties arise, particularly regarding these manufacturer's code specifications, because the position of each camera on the platform is opposite to the respective viewing direction (i.e., the oblique cameras look 'inward'); see Fig. 1.

(Gehrke et al., 2022) uses the term cardinal direction (East, North, South, and West) to define the direction of oblique cameras rather than associating these directions with the sensor installation orientation for adjustment computation for each oblique sub-block. This approach aligns each camera view with different cardinal directions depending on the flight path. However, the flight planning does not always align with the cardinal directions and may sometimes be rotated at an angle, such as 45 degrees from North (i.e., Northeast or Northwest). In these cases, this orientation is referred to as an intercardinal direction (Northeast, Northwest, Southeast, and Southwest). To avoid confusion and ambiguity in directional terms (which could be mistaken for left, right, forward, or backward), we propose the term *compass direction (CD)* as a more comprehensive frame of reference. This term encompasses all viewing directions, including cardinal directions, intercardinal directions, and any other orientations. Defining directions is crucial to avoid confusion between the viewing direction of images in object space and the mounting orientation of each camera on the platform. We are using compass directions over platform direction (PD), as this enhances clarity in discussions. When sensors collect data, the platform's view changes according to the flight direction. It has been observed that with each strip captured, the two opposite oblique cameras switch their view directions, while the compass direction remains constant, consistently aligning with the flight path (see Fig. 1). This approach ensures continuous and stable ground coverage, similar to the nadir camera, and facilitates easier interpretation and analysis.

Additionally, (ASPRS, 2024) introduces the best practices and guidelines for mapping with digital aerial oblique imagery, including relevant terminology and definitions. In this paper, we use the terms *far line* and *near line* for Maltese cross configurations, as suggested by ASPRS, to clarify our approach. The far line refers to the rearward-most edge of an oblique image (farthest from the camera station). Conversely, the near line indicates the leading edge (nearest to the camera station) of an oblique image. These terms denote the pair of edges in oblique images that are, respectively, farthest and nearest to the edge of the adjacent nadir image, enabling the computation of overlap measures for neighboring oblique images across track and along track, as shown in Figure 2.

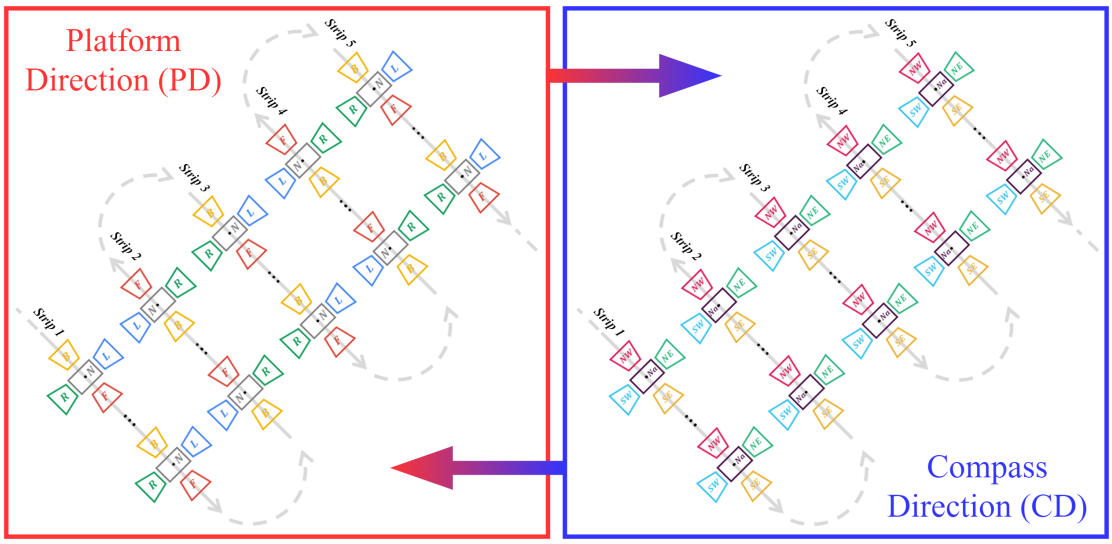

Manufacturer's design code	Installation Position on the platform	View looking
D	Right	Left-looking (L)
X	Back	Forward-looking (F)
A	Left	Right-looking (R)
W	Front	Backward-looking (B)
S	Middle	Downward-looking (N)

Strip
Strip 1, 3, 5 in (L) and Strip 2, 4 in (R)
Strip 1, 3, 5 in (F) and Strip 2, 4 in (B)
Strip 1, 3, 5 in (R) and Strip 2, 4 in (L)
Strip 1, 3, 5 in (B) and Strip 2, 4 in (F)
Strip 1, 2, 3, 4, 5 in (N)

Azimuth	Compass Direction
45°	Northeast (NE)
135°	Southeast (SE)
225°	Southwest (SW)
315°	Northwest (NW)
-	Nadir (Na)

Figure 1. Illustration of the penta-camera frame view directions: the red rectangle represents the platform direction (PD), and the blue rectangle represents the compass direction (CD).

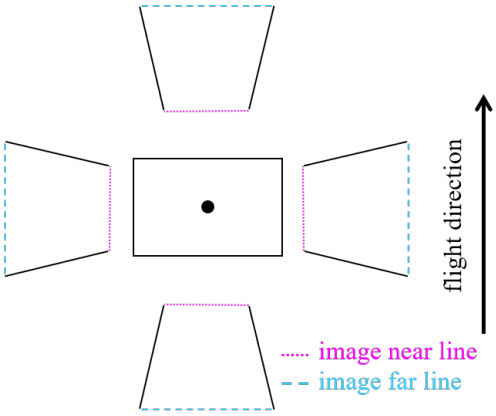

Figure 2. Illustration of the near line and far line of oblique images in the flight direction from a single exposure position.

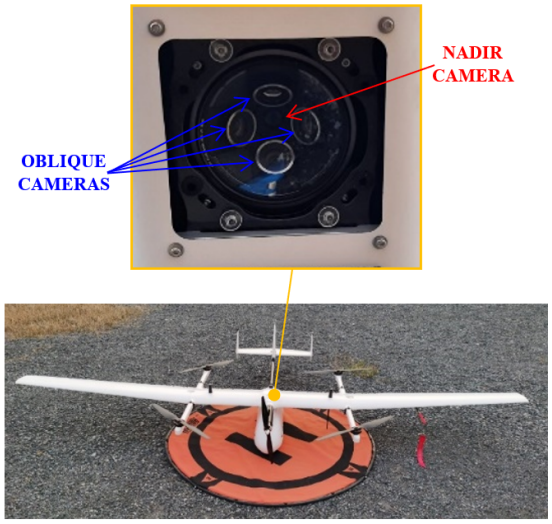

Figure 3. The VTOL UAV equipped with the JOUAV CA502R small-format multi-head camera system.

2. MATERIAL AND METHODS

2.1 Cameras

This study utilizes a "JOUAV CA502R" small-format multi-head camera system which is "designed for high-precision 3D mapping and surveying". The camera consists of one nadir and four 45-degree oblique cameras. Each of the five cameras in the system has a resolution of 24 MP (6000 x 4000), resulting in a combined total of 120 MP across the system. The nadir camera is equipped with a 28 mm focal length, while the oblique cameras each have a 43 mm focal length. The system was mounted on a VTOL UAV, as shown in Figure 3.

2.2 Survey and Study Area

The aerial survey was conducted over a 1.0 km² area in Saraburi Province, Thailand, using the VTOL UAV at an altitude of 150 meters above ground. The survey captured a total of 6065 images, averaging 1213 images per camera, with 80% overlap and side lap, referring only to the nadir image. The ground sampling distance (GSD) for the nadir view is 3 cm/pixel. The survey was supported by 48 ground control points (GCPs) measured with RTK-GNSS, achieving a mean positional accuracy of 5 cm. The

study area, including the distribution of GCPs, is illustrated in Figure 4.

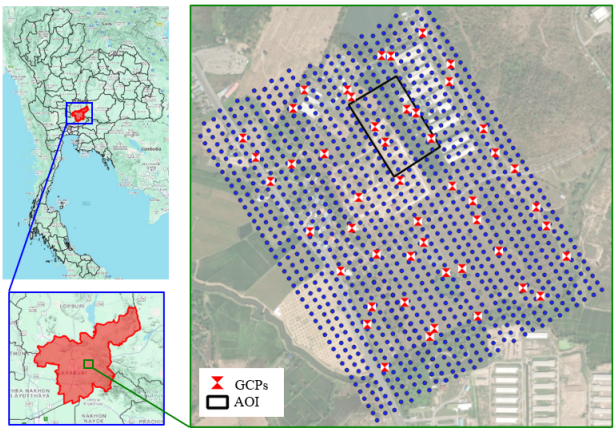

Figure 4. Distribution of control points within the study area and camera positions (blue circles); Area of Interest (AOI) for investigation in this paper (black rectangle).

2.3 Processing

The data is processed using OrientAL software (Karel et al., 2013), developed by the Department of Geodesy and Geoinformation at TU Wien, Austria. OrientAL implements a comprehensive Structure from Motion (SfM) pipeline that includes feature point extraction, description, and matching, along with gross error detection using essential matrix filtering with RANSAC (Fischler and Bolles, 1981). The software then performs an incremental bundle block adjustment to refine the image orientation. Additionally, OrientAL includes the capability to integrate observed control points into the bundle adjustment process and supports the modeling of multi-head camera systems, providing flexibility and precision in photogrammetric image orientation, camera calibration, and object reconstruction. These features ensure accurate and reliable processing of the captured images. Figure 5 represents image orientation with reconstructed sparse point cloud in model space.

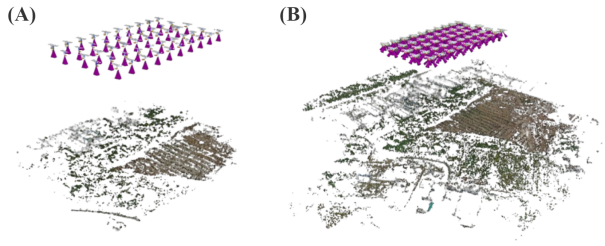

Figure 5. Image orientation with reconstructed sparse point cloud: (A) single-camera nadir, and (B) penta-camera.

3. RESULTS AND DISCUSSIONS

This section analyzes various computational factors, accuracy, and workflow optimization in both single-camera and penta-camera processing projects. Ground Control Points (GCPs) were used. We investigated an area of interest with 50 penta groups, arranged in 5 strips (10 penta groups per strip). The distance between neighboring penta groups within a strip (along track) is 25 meters, and 30 meters between neighboring strip penta groups (across track). We then compared the relative and interior orientation measures to the manufacturer's settings. We analyzed image connectivity, image ray intersection angle, and tie point multiplicity in this order. Image connectivity and image ray intersection angles reveal current limitations, while tie point multiplicity enables us to compute different scenarios and assess its impact on quality.

The accuracy comparison between single-camera (nadir) and penta-camera (nadir and oblique) processing, focusing on relative orientation, reveals that the sigma naught values of tie points are 0.78 pixels for single-camera processing and 0.81 pixels for penta-camera processing. Regarding the Root Mean Square (RMS) errors of GCPs, the use of oblique images notably improves accuracy, particularly in the vertical component, while planimetric accuracy remained consistent. When using all tie points, the horizontal RMS of the GCPs remains consistent at 0.020 m for both processing types, while the vertical RMS was 0.014 m for single-camera processing and slightly lower at 0.012 m for penta-camera processing. When excluding 2-fold tie points, the horizontal RMS of the GCPs remained stable at 0.020 m across both configurations, but the vertical RMS improved further, showing values of 0.014 m for single-camera processing and a refined 0.006 m for penta-camera processing. This enhanced vertical accuracy highlights a potential advantage of penta-camera configurations when omitting 2-fold tie points.

3.1 Image Connectivity

In this paper, image connectivity describes a property of image pairs: the number of corresponding points between them. It can be determined for any combination of two images. The question arises what an ideal distribution of image connectivity measures would be. Considering the limitation of IT resources (and while IT energy consumption occurs to a large share in data centers and for other tasks than image orientation), the number of tie points needs to be limited for very large bundle blocks. Independent thereof, it is worth striving for precise and unbiased estimates of orientation parameters obtained within short time. A starting point could be to aim at an image connectivity (in the above sense) which is proportional to the overlapping area of any image pair (measured in image space). This follows the concept of "von Gruber" areas. However, the influence of variations in image texture and quality is not considered in this formulation.

To analyze image connectivity, measures can be aggregated in various ways, such as by camera type (e.g., all nadir images with all NW looking images) or for image pairs that consistently have the same geometric configuration in a strip (e.g., each nadir image with the SW looking image three exposures later). In this study, we base our analysis on the compass direction frame. Figure 6 shows the image connectivity matrix of the penta-camera. Within the matrix, each image contributes to one row and one column, ordered by compass direction, with images sharing the same direction grouped into distinct rows and columns. Each direction in the block matrix consists of a 50 by 50 grid, with light gray lines separating every 10 by 10 grid to distinguish each strip, resulting in a total of 5 strips per block matrix. For example, the 1^{st} NE looking image of the 1^{st} strip connects with approximately the 5^{th} image of the same strip and then again with approximately the 18^{th} image (equivalent to the 8^{th} image of the 2^{nd} strip). The colors in the block image connectivity matrix represent the number of corresponding points between image pairs on a logarithmic scale, with the

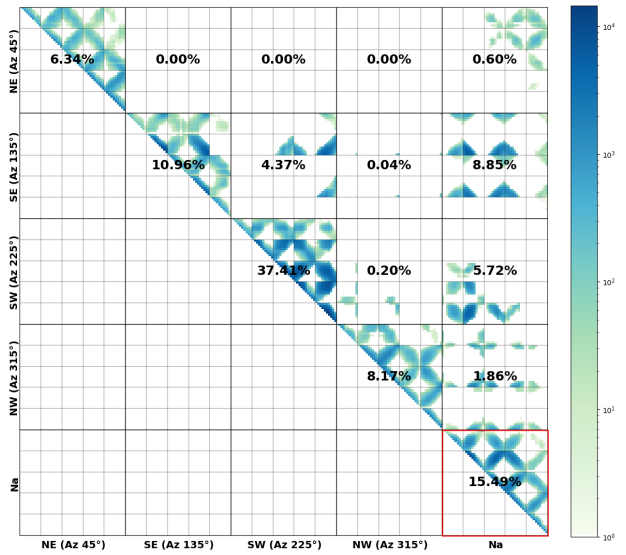

Figure 6. Image connectivity of the penta-camera in the compass direction frame (log scale). The center of each block matrix shows the percentage of corresponding points within and across view directions.

	NE	SE	SW	NW	Na
NE	308 | 2361	0 | 0	0 | 0	0 | 0	69 | 355
SE		294 | 10380	813 | 4419	153 | 503	770 | 5805
SW			1861 | 14615	114 | 452	511 | 5062
NW				419 | 2930	164 | 1769
Na					817 | 8786

same direction	90°difference	180°difference	CD with nadir

Table 1. Count of corresponding points between image pairs across the different compass view directions (75th percentile | maximal), indicating image connectivity

percentage of corresponding points displayed at the center of each block in the matrix. Additionally, Table 1 presents a matrix of the number (75th percentile | maximum) of corresponding points between image pairs across the different compass view directions. Each cell in this table corresponds to a block in the matrix shown in Fig. 6. We classified the view directions into four groups (indicated by colors in Table 1): same view direction (yellow), 90-degree difference in view direction (blue), 180-degree difference in view direction (green), and compass direction with nadir (red). The diagonal of the matrix represents pairs with the same view direction. All five same-view direction pairs exhibit a similar density pattern, consistent with the side lap and overlap defined in the flight plan.

Considering the Na-Na matrix (red rectangle in Fig. 6), which corresponds to the same matrix in the case of single-camera processing, each strip can be observed in intervals of 10 cells. The presence of color in 3-4 consecutive cells, both along track and across track, indicates that these images have corresponding points or an overlap of approximately 80% with each other. This confirms that the nadir camera's overlap and side lap percentages adhered to the planned configuration. Further analysis shows that these parameters influence the overlap for oblique cameras when calculating the oblique overlap frame's percentage based on the nadir frame's percentage overlap. When consider neighboring strip image pairs (across track), the overlap of NW and SE looking images decreases to a minimum of 68% at the near line and gradually increases to around 80% at the far line. Typically, the standard overlap and side lap for airborne cameras are designed to be at least 60% to ensure homogeneous accuracy. For neighboring images within the strip (along track) for the NE and SW looking images, the overlap ranges from 80% at the near line to 85% at the far line. This confirms that there are no gaps at the near line between overlapping frames in each individual compass direction. Therefore, both the nadir and oblique cameras have a high overlap, which is beneficial for image processing. However, the 80% of overlap and side lap for the nadir images do not result in the same symmetry in the oblique image overlaps. Such a symmetric overlap could be considered desirable for enhancing the visibility of facades in oblique images.

For the 90-degree and 180-degree difference in view direction, some image pairs show fewer corresponding points compared to pairs looking in the same direction (yellow), including the compass direction with nadir view direction. Table 1, which shows the 75th percentile and maximum number of corresponding points, indicates that the SW-SW direction has the highest number of corresponding points among all directions, approximately twice that of the Na-Na. For a block matrix with a value of zero, this means that no matching points were found.

Various factors may contribute to these results, such as geometric design, the percentage of overlap and side lap, the texture of the captured land use, and the size of the processing area. Since this study investigated an area of interest where the length and width are not equal, it leads to variability in the values shown in the matrix and cells. It is, however, obvious that the differences in image connectivity deviate strongly from the proportionality to image overlap.

3.2 Image Ray Intersection Angle

The image ray intersection angle refers to the angles formed by the lines of sight from two or more camera positions to a 3D point, which affects the precision of spatial measurements. For the cameras investigated, we derived the theoretical intersection angles and compared them to the actual intersection angles achieved. Figure 7 shows the theoretical intersection angles of all possible directional pairing between two points of exposure. The possible maximum intersection angles between nadir-to-nadir, oblique-to-oblique, and nadir-to-oblique pairs are 46, 110, and 78 degrees, respectively.

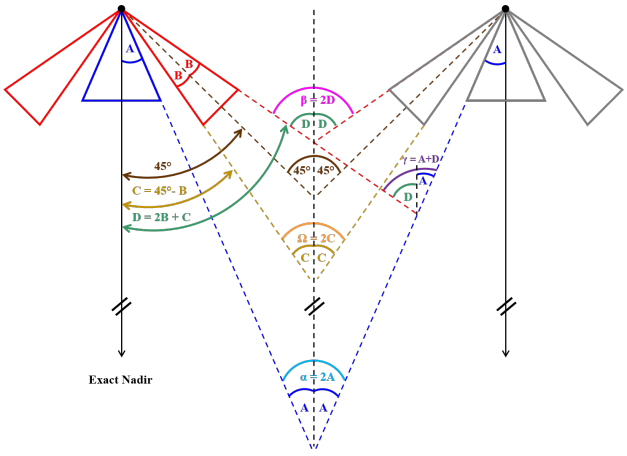

Figure 7. Intersection angles based on platform geometry.

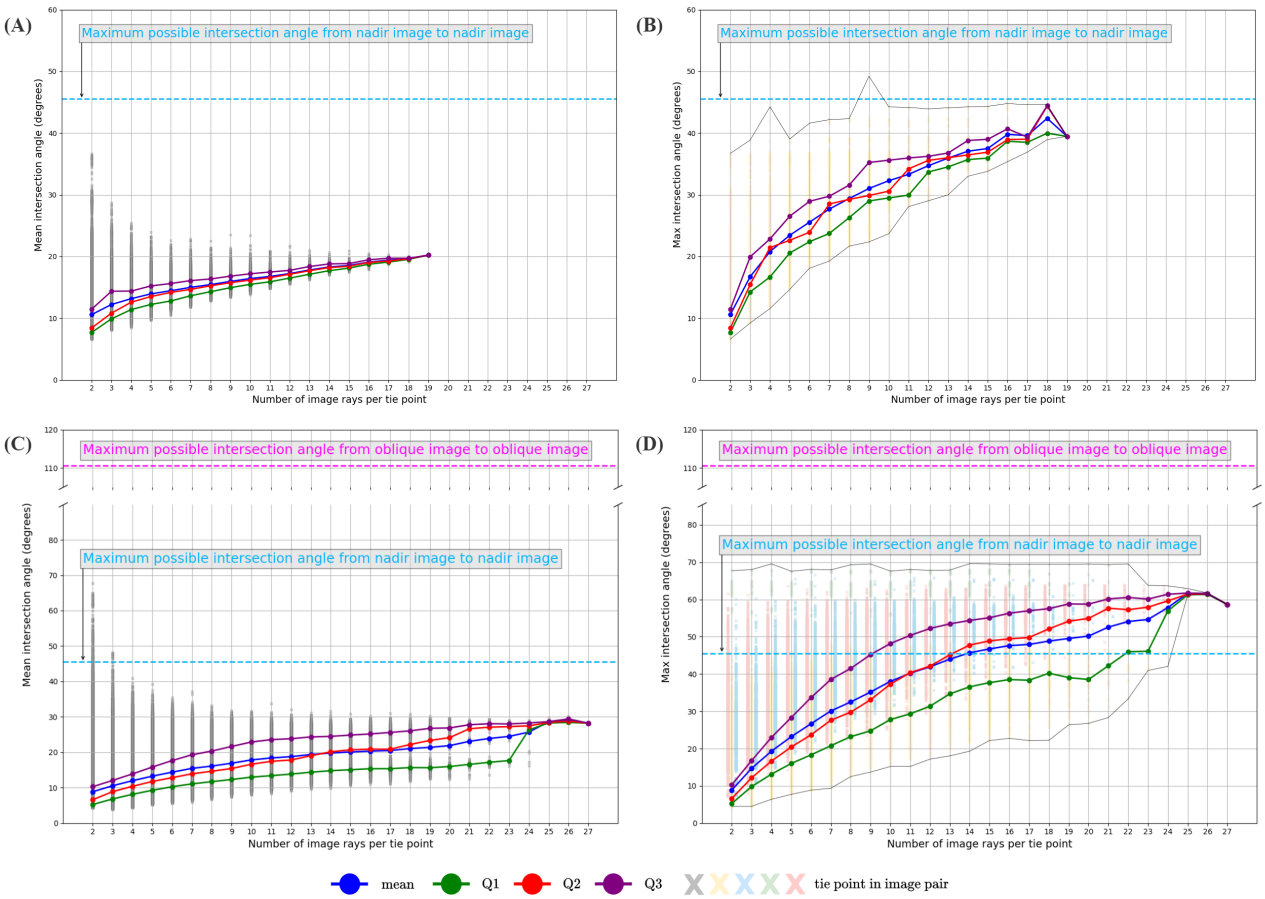

Figure 8. Mean and maximum image ray intersection angles for each tie point in the project: (A) Mean intersection angle for single-camera processing (B) Maximum intersection angle for single-camera processing (C) Mean intersection angle for penta-camera processing (D) Maximum intersection angle for penta-camera processing

All rays to one tie point are used pairwise to compute the angle between the rays. For each tie point, the average and the maximum of these angles is selected for the further analysis. Figure 8 shows the mean and maximum intersection angles for each tie point, with statistical values (mean, 25^{th}, 50^{th}, and 75^{th} percentiles) for both processing types. The mean intersection angle is represented in grey, while the maximum intersection angle uses the same color scheme as in Table 1 from section 3.1. The mean intersection angle (in Fig. 8A and 8C) shows that tie points observed in two images have an intersection angle around 10 degrees, which rises to about 20 degrees as the number of images observing each point increases. This suggests that, for most tie points, the mean intersection angle ranges from 10 to 20 degrees, even 30 degree in case of nadir and oblique combined.

For the max intersection angle, in the single-camera processing (in Fig. 8B), all tie points have maximum intersection angles below the theoretical maximum nadir-to-nadir angle, except for one point due to incorrect matching. In the penta-camera processing (in Fig. 8D), all tie points fall below the theoretical maximum oblique-to-oblique angle. By analyzing the color range associated with different angles, we observe that as the angle increases, the different image pairs are contributing (as expected). This is visualized through a color scheme: tie points from the same view direction typically have small maximum intersection angles, represented in yellow. Points in the compass direction with nadir exhibit higher maximum angles, shown in red. Points with 90-degree differences appear in blue, and those with 180-degree differences are within the highest angle range, displayed in green. Overall, the results are consistent with the theoretical intersection angles. Additionally, the two thin black lines in Fig. 8B and 8D show the overall minimum and maximum intersection angle. This confirms that the actual flight was following the plan (particularly w.r.t. to pitch and roll angle) and that wrong matches between image points do not go beyond this bound. The fact that the actual maximum intersection angles per tie point are well below the theoretically possible maximum intersection angles indicates a moderate exploitation of the accuracy potential offered by oblique images, especially w.r.t. elevation accuracy.

3.3 Tie Point Multiplicity

Tie point multiplicity refers to the number of images contributing to the calculation of a 3D point, indicating how many times a point has been measured across different images. Figure 9 shows the tie point multiplicity, highlighting the number of tie points. This reveals a significant dominance of 2-fold tie points, which form the largest group in both processes. In high-overlap UAV blocks with many images, numerous tie points have similar viewing directions. This raises the question of whether removing these tie points from the bundle block adjustment could reduce the number of unknowns without compromising quality, thereby increasing accuracy and reducing processing time. Further analysis show that tie points appearing in only two images do not contribute much to improving efficiency in image orientation or camera calibration because they are not controlled

along their epipolar line and are, therefore, less reliable.

Additionally, statistics of the image residuals are shown in Figure 9. In single-camera processing, there is considerable variation, whereas in penta-camera processing, these values remain more stable. The blue area between $\pm$ 0.2 pixels highlights the trend of image residual (μ_x and μ_y) for both processing types. The purple lines in Fig. 9 show the length of the residual vector per tie point, specifically showing the group-wise average for tie points of the same multiplicity. As expected, this line grows sharply from the 2-fold tie points and appears to converge for larger multiplicity, excluding the averages of residual length vectors based on very few samples for very high multiplicity. The dashed line shows the actual mean residual lengths obtained from the bundle block adjustment, whereas the solid line results from simulation. For this end, image measurements were made error free by adding the residual to the measurement. A bundle block adjustment of these "corrected measurements" estimates all residuals to be zero. Adding random measurement errors to these "corrected measurements" drawn from a normal distribution with a mean value zero and a standard deviation of sigma naught of the original adjustment estimates new residuals which are only affected by random errors. The sigma naught of these adjustments with the original observations were 0.78 pixel for the block of nadir images only and 0.81 pixel for the block with both nadir and oblique images. We observed that the plotted line from the bundle block simulation, showing the expected residual length per multiplicity, fits perfectly to the shape of $\frac{1}{m}\left(\sigma \cdot \sqrt{\frac{\pi}{2}}(m-2) + \sigma \cdot \sqrt{\frac{2}{\pi}}\right)$, where m is the number of images and σ is the image coordinate measurement precision.

We also noted that the average residual, grouped by tie point multiplicity, is closer to the expected value of zero for the penta-camera setup. However, the deviations from zero for the single camera case are very small (0.05 pixel).

These results indicate that some of the assumptions of the adjustment (correct functional and stochastic model, e.g. independent observations of homogeneous accuracy, constant interior orientation per camera, etc.) are not fully met.

4. CONCLUSIONS AND OUTLOOK

In this paper, we investigate the computational factors that affect the performance of small-format multi-head camera systems. We propose using the compass direction (CD) frame as a superior reference frame to avoid confusion regarding oblique cameras and oblique viewing directions, as it facilitates continuous and consistent ground coverage, similar to the nadir camera. This frame significantly helps in focusing interpretation and discussion.

Our findings reveal that image connectivity significantly deviates from being directly proportional to image overlap. Although the flight plan for data collection was designed with a high overlap and side lap of 80% for the nadir camera, these parameters influence the overlap for oblique cameras. While, there are no gaps at the near line between overlapping frames in each individual compass direction, the nadir images overlaps do not lead to the same symmetry in the oblique image overlaps. Achieving such symmetry could enhance the visibility of facades in oblique images. For the image ray intersection angle, the results show that the overall maximum intersection angles are consistent with the theoretical values, confirming that the actual flight was following to the planned parameters. However, the observation that maximum intersection angles per tie point remain well below theoretically possible values indicates a moderate exploitation of the accuracy potential offered by oblique images. In terms of tie point multiplicity, the results show that the residual vector length per tie point deviates from expectations (based on normally distributed image point errors with the very same standard deviation), suggesting that some underlying assumptions in the adjustment model were unmet. Additionally, by adding the oblique images to the nadir image block and removing the 2-fold tie points, the sigma naught increases slightly from 0.78 pixels to 0.81 pixels. However, the vertical residuals of the GCPs decrease from 1.4 cm to 0.6 cm, while planimetric accuracy remains stable. Thus, incorporating oblique images and omitting the 2-fold tie points are beneficial for increasing height accuracy.

The results indicate directions for improvement. The camera setup is not yet fully optimized. In future work, bundle block adjustment will be applied to entire datasets to assess its impact on various computational factors in general mapping. Additionally, further evaluations of relevant factors, such as camera calibration and the number and distribution of GCPs, will be undertaken.

ACKNOWLEDGMENT

The authors express their gratitude to the Department of Survey Engineering, Faculty of Engineering, Chulalongkorn University, and N.P. Survey Company Limited, Thailand, for supporting the dataset used in this research.

REFERENCES

Alsadik, B., Remondino, F., Nex, F., 2022. Simulating a Hybrid Acquisition System for UAV Platforms. *Drones*, 6(11). https://www.mdpi.com/2504-446X/6/11/314.

ASPRS, 2024. ASPRS Positional Accuracy Standards for Digital Geospatial Data. June, 24. https://publicdocuments.asprs.org/PositionalAccuracyStd-Ed2-V2.

Bannakulpiphat, T., Santitamnont, P., 2024. A Comparative Analysis of Camera Rig Parameters in Photogrammetric Software for Small-Format Oblique Camera System on Unmanned Aerial Vehicle. *International Journal of Geoinformatics*, 20(2).

Fischler, M. A., Bolles, R. C., 1981. Random sample consensus: a paradigm for model fitting with applications to image analysis and automated cartography. *Commun. ACM*, 24(6), 381–395. https://doi.org/10.1145/358669.358692.

Gehrke, S., Müller, M., Kukla, M., Beshah, B., 2022. Hierarchical Aerial Triangulation of Oblique Image Data. *The International Archives of the Photogrammetry, Remote Sensing and Spatial Information Sciences*, XLIII-B2-2022, 45–50. https://isprs-archives.copernicus.org/articles/XLIII-B2-2022/45/2022/.

Karel, W., Doneus, M., Verhoeve, G., Bries, C., Ressl, C., Pfeifer, N., 2013. ORIENTAL - Automatic Geo-Referencing and Ortho-Rectification of Archaeological Aerial Photographs. *ISPRS Annals of the Photogrammetry, Remote Sensing and Spatial Information Sciences*, II-5/W1, 175–180. https://isprs-annals.copernicus.org/articles/II-5-W1/175/2013/.

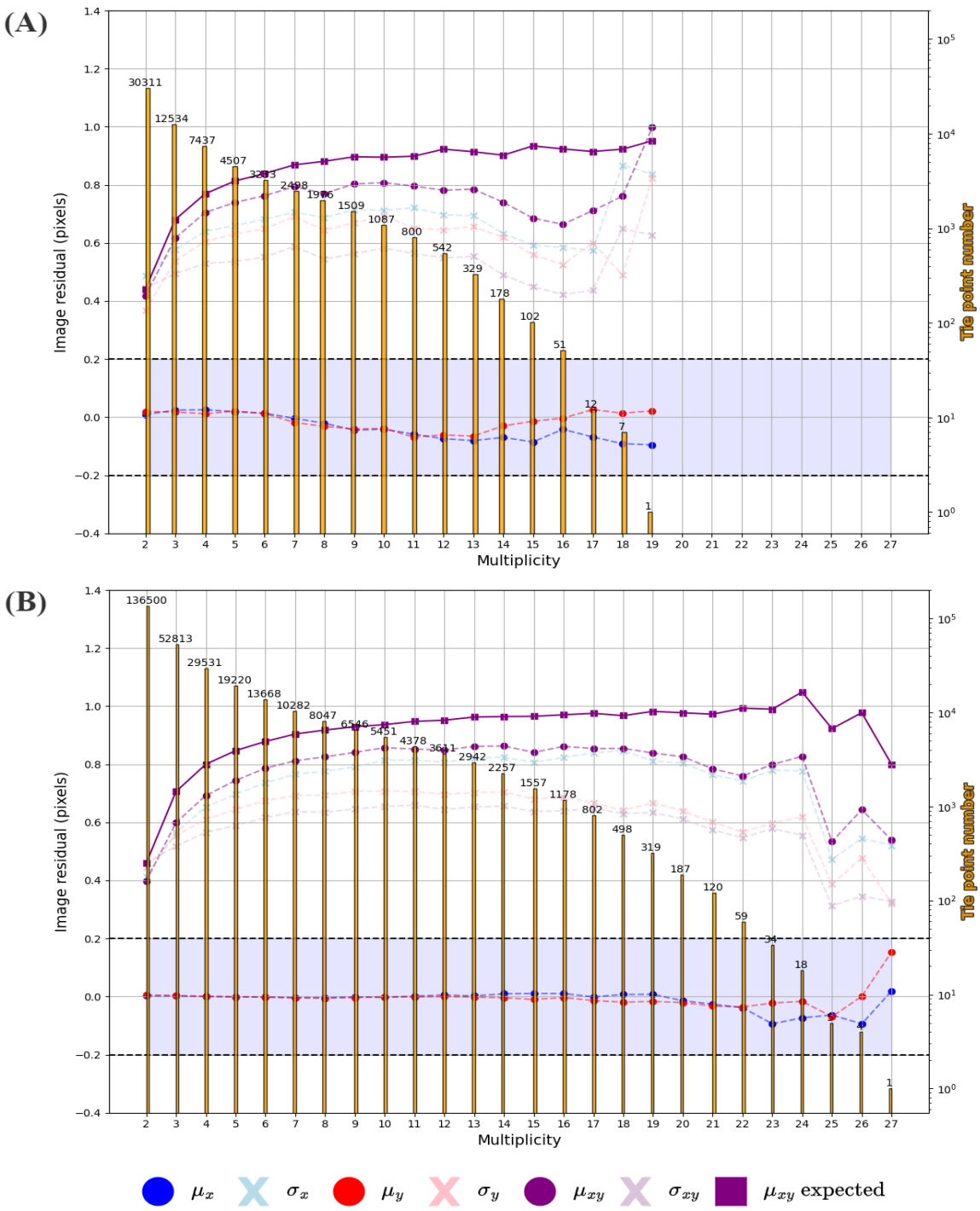

Figure 9. Tie point multiplicity with statistics of the image residuals: (A) single-camera, (B) penta-camera.

Maset, E., Magri, L., Fusiello, A., 2024. Principled bundle block adjustment with multi-head cameras. *ISPRS Open Journal of Photogrammetry and Remote Sensing*, 11, 100051.

Nex, F., Armenakis, C., Cramer, M., Cucci, D., Gerke, M., Honkavaara, E., Kukko, A., Persello, C., Skaloud, J., 2022. UAV in the advent of the twenties: Where we stand and what is next. *ISPRS Journal of Photogrammetry and Remote Sensing*, 184, 215-242.

Remondino, F., Gerke, M., 2015. Oblique aerial imagery : a review. D. Frietsch (ed.), *Proceedings of Photogrammetric Week '15, 7-11 September, Stuttgart, Germany*, Wichmann, 75–83.

Toschi, I., Ramos, M. M., Nocerino, E., Menna, F., Remondino, F., Moe, K., Poli, D., Legat, K., Fassi, F., 2017. Oblique Photogrammetry Supporting 3D Urban Reconstruction of Complex Scenarios. *The International Archives of the Photogrammetry, Remote Sensing and Spatial Information Sciences*, XLII-1/W1, 519–526. https://isprs-archives.copernicus.org/articles/XLII-1-W1/519/2017/.

Verykokou, S., Ioannidis, C., 2020. Exterior orientation estimation of oblique aerial images using SfM-based robust bundle adjustment. *International Journal of Remote Sensing*, 41(18), 7233–7270. https://doi.org/10.1080/01431161.2020.1755737.